

ELECTROKINETIC FLOW INSTABILITIES IN MICROFLUIDIC SYSTEMS

Hao Lin, Michael H. Oddy and Juan G. Santiago

Mechanical Engineering Department, Stanford University

Stanford, CA 94305, USA

juan.santiago@stanford.edu

Abstract The stability of electrokinetic flow in a rectangular cross-section microfluidic channel with transverse conductivity gradients and driven by streamwise electric fields was explored. Such a system exhibits a critical electric field above which the flow is highly unstable, resulting in fluctuating velocities and rapid stirring. The problem was studied using theoretical and numerical analyses, as well as experimental observations. It was found that the internally generated electric body force was responsible for the instability, whereas the diffusion of ion species provided a stabilizing mechanism. Various models including two-dimensional and depth-averaged formulations were studied; modeling results compare well with experimental observations. These results have application to the design and control of on-chip assays that require high conductivity gradients, and provide a rapid mixing mechanism for low Reynolds number flow in microchannels.

Keywords: Electrokinetics, electrokinetic instability, critical electric field, electric conductivity gradient, microfluidics, microchannel, micromixing

1. Introduction

Over the past decade there has been an extensive research into the design of devices that perform chemical analysis in micro-fabricated fluidic channel structures. Often referred to as Micro Total Analysis Systems (μ TAS), these systems exhibit a mass transport regime that is often different from that of macro-scale flow devices. Many of these devices apply electrokinetic liquid-phase, bioanalytical techniques including capillary electrophoresis and isoelectric focusing, and often manipulate the samples having poorly characterized or unknown electrical conductivi-

ties. As a result, conductivity mismatches often occur between the sample/reagent species and the background electrolyte. In the presence of applied electric fields, conductivity gradients can induce electrohydrodynamic coupling, which can in turn generate complex, unstable flow-fields. Flows exhibiting these physics have been reported in the classical electrohydrodynamics literature (see for example, the seminal paper by Hoburg and Melcher, 1976, and a later work by Baygents and Baldessari, 1998). In this paper, we review flow instabilities due to electric field and conductivity gradients coupling in electrokinetic systems. Electrokinetic flows are a subset of electrohydrodynamics characterized by the presence of an electrical double layer and regimes, where transport due to molecular diffusion is important.

Although desirable for rapid-mixing applications, the electrokinetic instabilities are unwanted in microfluidics applications such as sample injection, separation, and controlled diffusion-limited reaction processes where minimal sample dispersion is required. This motivates research toward a better understanding of the conditions necessary for the onset of electrokinetic flow instability. In 2001 Oddy et al. first reported observation of electrokinetic instability (EKI) in a microchannel system. These experiments were performed in 4-mm-long glass capillaries with rectangular cross-sections, and the instabilities were in general of temporal nature (Oddy et al., 2001). In a slightly different geometry (microfluidic T-junction), Chen and Santiago also reported spatial amplification of disturbances which was later identified as convective instability (Chen and Santiago, 2002, Chen et al., 2004). In all of these experiments, conductivity gradients were in the spanwise direction (perpendicular to the electric field), and there existed critical values of the applied streamwise electric field above which instabilities and significant stirring occurred.

Following these initial experimental observations, there has been a development of models for electrokinetic flow instabilities. Models are useful in predicting threshold conditions for instability onset as well as other flow features including coherent wave structures and mixing rate. Lin et al. (2004) and Chen et al. (2004) showed that a generalized EHD modeling framework (derived from the so-called “leaky dielectric” model first developed by Melcher and Taylor, 1969) can be used to describe both the low-conductivity, non-diffuse charge dynamics of classical EHD, and the more recently reported flow instabilities of high-conductivity electrolyte in electrokinetic microsystems. Lin et al. (2004) analyzed the temporal stability properties based on a two-ion model, comprising the conductivity transport equation along with the conservation of momentum and electromigration current. They showed that the model provided good qualitative and fair quantitative agreement with regard to

the threshold electric fields and critical wavenumbers. Lin et al. (2004) also presented non-linear simulations of their set of governing equations that capture the high Peclet (or the so-called electric Rayleigh) number stirring events observed in experiments. Using a convective framework, Chen et al. (2004) showed that EKI could manifest itself convectively in the presence of a strong electroosmotic flow. In the latter analysis, EKI is modeled using a linearized, thin-layer limit of the Navier-Stokes equations coupled with conservation equations for electrical conductivity and current. The model reveals both convectively and absolutely unstable eigenmodes. More recently, Storey et al. (2004) presented a depth-averaged version of the governing equations used by the Lin et al. (2004) model. Their depth-averaged model compared favorably with a complete three-dimensional model for thin channel geometries.

In this paper we present our experimental, analytical, and computational results and some progress in the pursuit of modeling and understanding of EKI in electrokinetic microchannels. We shall briefly introduce the experimental results, followed by a general theoretical formulation developed in Lin et al. (2004). Using these equations we show the results from various linear analyses as well as nonlinear simulations, and assess their qualitative and quantitative agreements with experimental data. We conclude the paper by introducing our latest development in a depth-averaged framework suitable for the study of generalized electrokinetic flows in microchannels with thin channel geometry.

2. Experimental Observations

Here we show a few exemplary results from our experiments. The microchannel consisted of a borosilicate glass capillary (Wilmad-Labglass, NJ) with a rectangular cross-section. The channel was 4 mm long (in the x or streamwise direction), 1 mm wide (in the y or spanwise direction), and 0.1 mm deep (in the z or depth direction). Two buffer streams initially occupied the upper and lower halves of the microchannel, resulting in a diffuse conductivity gradient along the spanwise, y -direction; an electric field was subsequently applied along the streamwise, x -direction. The conductivity of the buffer streams were 50 and 5 $\mu\text{S}/\text{cm}$, respectively, resulting in a conductivity ratio of $\gamma = 10$. For flow visualization, an electrically neutral, heavy-molecular-weight dye (70 kDalton) composed of a dextran-rhodamine B conjugate (Molecular Probes, OR) was added to the high-conductivity buffer stream. The imposed electric potential initiated an electroosmotic flow in the channel and, for electric fields above a threshold value, electrokinetic instabilities.

A representative set of images from experiments conducted at 1, 2, and 3 kV applied potentials are shown in Fig. 1. The potentials were applied over a distance of 40 mm, such that they were equivalent to applied fields of 25,000, 50,000 and 75,000 V/m, respectively. In each case, the top figure of each series shows the initial, undisturbed interface between the dyed and undyed buffer streams in the channel ($t = 0$). The successive images in each column show the temporal evolution of the imaged dye under a constant, DC potential. In this color scheme, blue corresponds to the undyed, low-conductivity stream, and red to the dyed high-conductivity stream. For an applied field of 25,000 V/m, the interface was only slightly perturbed and only slight fluctuations are apparent in the images captured at 4.0 s and 5.0 s. At the two higher applied voltages, the interface exhibited a rapidly-growing wave pattern within the first 1 s. The unstable fluid motion in the channel buckled the interface and proceeded to stretch and fold the material lines. The transverse

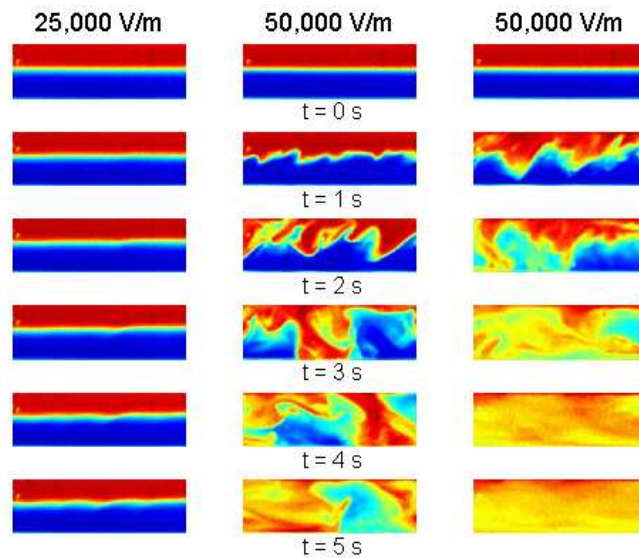


Figure 1. Sample images from the experiment, shown for applied fields of 25,000, 50,000, and 75,000 V/m, corresponding to the first, second, and third column. Images obtained at various times are shown for each column. The electric field and bulk flow directions were from left to right. High voltage was applied as a Heaviside function at $t = 0$ s. Each image corresponds to a physical area 1 mm wide (y) and 3.6 mm long (x). The depth of the channel is $100\ \mu\text{m}$ along the z -direction (into the page). Small amplitude waves at $t = 1$ s grew and led to rapid stirring of the initially distinct buffer streams. The instability stretched and folded material lines and, after about 4 s for the 75,000 V/m applied field, resulted in a well-stirred, relatively homogeneous dye concentration field. The time of the images in each row are shown in the figure.

and fluctuating velocities associated with this unstable motion resulted in rapid mixing of the two streams. At the 75,000 V/m applied field, the channel reached a well-stirred state and with nearly-homogeneous concentration fields observable within 5 s.

3. Formulation

The description of experiments given above serves as an introduction to the problem and describes the observed features of electrokinetic flow instability. We now turn to a theoretical formulation of the flow. In this section, we summarize the governing equations and discuss the parameters of interest in our experiment. The equations of our model are derived from the conservation laws for a dilute, two-species electrolyte solution (Probstein, 1994), and we have adopted (with justification) a relaxation assumption to simplify the equations. The scaling analysis and derivations are discussed in detail in Lin et al. (2004) and should not be repeated here. The (*dimensionless*) equations read

$$\frac{\partial \sigma}{\partial t} + v \cdot \nabla \sigma = \frac{1}{\text{Ra}_e} \nabla^2 \sigma, \quad (1)$$

$$\nabla \cdot (\sigma \nabla \Phi) = 0, \quad (2)$$

$$\nabla^2 \Phi = -\rho_E, \quad (3)$$

$$\nabla v = 0, \quad (4)$$

$$\text{Re} \left(\frac{\partial v}{\partial t} + v \cdot \nabla v \right) = -\nabla p + \nabla^2 v - \rho_E \nabla \Phi, \quad (5)$$

where σ is the conductivity, v is the bulk fluid velocity, Φ is the electric field (which includes both the applied and generated components), and p is pressure. The electric Rayleigh number (similar to the Peclet number) and the Reynolds number that arise from the nondimensionalization are defined as

$$\text{Ra}_e \equiv \frac{U_{ev} H}{D}, \quad \text{Re} \equiv \frac{U_{ev} H}{\nu}.$$

Here H is half-channel width, D is an effective diffusivity of the conductivity, and ν is the kinematic viscosity of the electrolyte solution (usually aqueous). The velocity U_{ev} , the so-called electroviscous velocity, is velocity scale derived by setting equal the electric body force and the viscous force in the momentum equation. (See Hoburg and Melcher, 1976, Lin et al., 2004 and Chen et al., 2004; more discussions on these parameters can also be found in these references.)

4. Two-dimensional Model

We first present a model where we assume that the flow exists only in the $x - y$ plane, and that there is no dynamics in the z -direction. This analysis will capture the basic physics of the instability mechanisms due to the conductivity gradient.

We first use a linear stability analysis to predict the regimes where we would expect rapid mixing to occur. The base states are a diffused, spanwise conductivity profile $\sigma_0 = \sigma_0(y)$ with a (high-to-low) conductivity ratio of 10, and a shear electroosmotic flow $u_0 = u_0(y)$. Note that the spanwise dependence of the latter was induced by that of the former *via* the dependence of zeta potential on conductivity.

We assume that disturbance is periodic in the x direction, and the growth of amplitude is exponential in time. We have obtained, for each streamwise wave number k and applied field E_0 , a set of eigenvalues (the exponential growth rates), together with their respective eigenfunctions. In Fig. 2 we show a contour plot of the growth rates of the most unstable eigenfunction in the wave number-Rayleigh number (electric field) parameter space. Symbol s denotes the real and dimensional growth rate. The neutral stability curve is obtained by setting $s = 0$. A threshold electric field is successfully captured from the minimal value of E_0 on the neutral stability curve. As originally reported by Baygents and Baldessari (1998), we found that the inclusion of the diffusive term $\nabla^2 \sigma / \text{Ra}_e$ in Eq. (1) is crucial for the existence of the neutral stability curve.

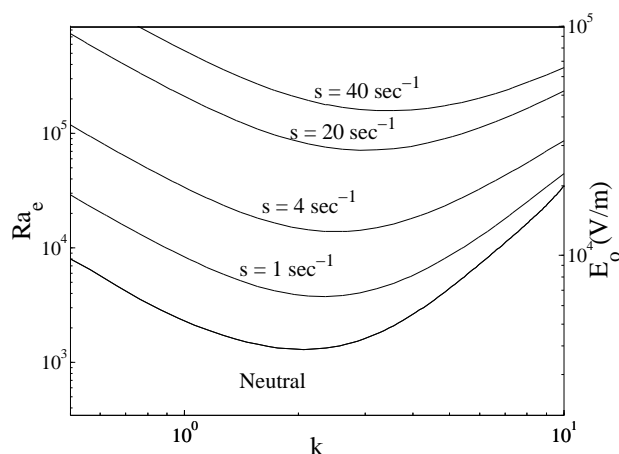


Figure 2. Contour plot of growth rates (s) versus wave number and Rayleigh number. Dimensional applied electric field is provided on the right-hand axis. For the case plotted here, the ratio of the conductivity between the two streams is 10.

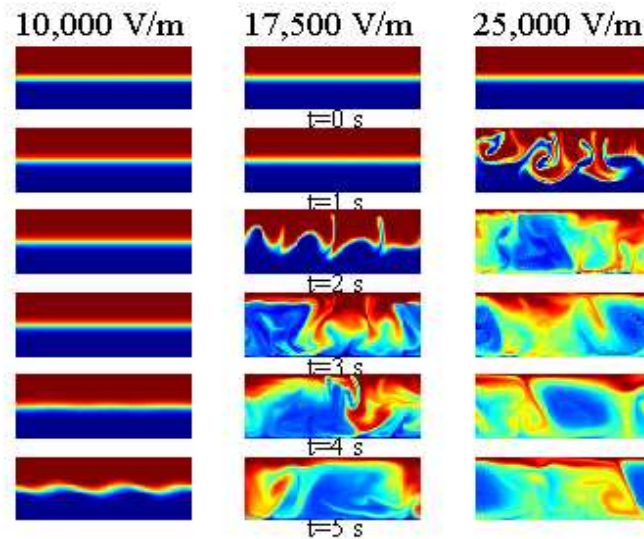


Figure 3. Snapshots of the simulated dye field at various instances in time for different driving electric fields. In this color scheme red corresponds to the high conductivity buffer, and blue to the low one. Each column indicates a different applied field and the rows within each column present the selected snapshots in time. The image corresponds to a physical domain of $3.6\text{ mm} \times 1\text{ mm}$. The time for noticeable waves to develop is decreased as the field is increased.

In addition to the two-dimensional linear stability analysis presented above, we have also solved the full nonlinear governing Eqs. (1-5) numerically to capture the nonlinear evolution of the instability observed in the experiments. The initial conditions are the base states plus a small white noise perturbation. The solution details are documented in Lin et al. (2004). Figure 3 shows the nonlinear evolution of the simulated dye at various instances in time and for three different electric fields. The model reproduces many of the essential features observed in the experiments, including the shape and initial break-up dynamics of the interface, the transverse growth of a wave pattern in the interface, and the roll-up of scalar structures observed at later times. Note the similarity in the most unstable (and most apparent) wave number at later times between the simulation and experiments.

Despite the similarities between the wave number and dynamics of the interface breakup, the threshold imposed fields from both the linear and nonlinear predictions are lower than those shown for the experiment in Fig. 1. For example, compare the evolution of the dye at $25,000\text{ V/m}$ from the experiments (Fig. 1, column 1) and the simulation (Fig. 3, column 3). We see that the simulation at $25,000\text{ V/m}$ predicts

a well-stirred flow field in less than three seconds, while experiments show that the flow is stable on the time-scale of the experiments. The simulation of 25,000 V/m is qualitatively similar to the experimental flow at 75,000 V/m (Fig. 1, column 3). Despite the discrepancy in the magnitude of the applied field, our simulation captures a threshold field and scalar features qualitatively similar to the experiment. In the following section we address possible causes for the under-prediction of the threshold electric field by including three-dimensional effects.

In comparison with the temporal instability analysis presented here (which is consistent with the experimentally observed instability in the previous section), Chen et al. (2004) analyzed the instability in a convective framework which is consistent with the spatial growth that was observed in T-junction microfluidic channels. Among other contributions, the authors found that an important dimensionless group R_ν , defined as the ratio of the electroviscous to electroosmotic velocity, is critical in demarcating the absolute/convective instability boundary. Interested readers are referred to Chen et al. (2004).

5. Depth-averaged Model

In the previous sections we have provided a two-dimensional framework which appears to capture the primary physics of our flow. However, the primary flaw in that model is the two-dimensional assumption, for a channel with an aspect ratio of $\delta \equiv d/H = 0.1$, where d denotes the channel half-width. Such a thin channel geometry was also used in the experimental work of Chen et al. (Chen et al., 2002; Chen et al., 2004). In three dimensions, an EDL forms not only on the top and bottom walls of $y = \pm 1$, but also along the side walls ($z = \pm 1$), and strongly drives the flow due to the small depth of the channel. The three-dimensional nature of a thin channel has the added dynamics that the fluid motion in the interior of the channel is directly coupled to the top and bottom wall boundary condition (determined in part by the local value of ion density).

In Lin et al. (2004) we presented a 3D linear analysis and found that the predicted threshold field was one order-of-magnitude higher than that from the 2D linear analysis, in much closer agreement with the experimental observations. However, a depth-averaging approach is preferred since in general, the 3D analysis (simulations) are computationally more expensive, and considering that the microchannels of our interest are “shallow” in the depth (z) direction. In Chen et al. (2004) a depth-averaged analysis was performed on a set of linearized governing equations and the resulted linear equation system was used for convective

instability analysis. In Storey et al. (2004) a more complete Hele-Shaw type of integrated momentum equation was used. Both models yielded favorable quantitative results when compared with experimental data.

Here we extend and complete the ideas that were first developed by Chen et al. (2004) and Storey et al. (2004). We develop a generalized, nonlinear depth-averaged model suitable for the study of electrokinetic microchannel flows with thin channel geometries. We accomplish this through a complete asymptotic analysis of the full three-dimensional equations based on a smallness parameter which is the channel cross-sectional aspect ratio δ . Our general methodology follows a combined lubrication (for the momentum equations) and Taylor-Aris (for the convective-diffusion of the conductivity field) approach. Without presenting the details of the derivation, we list the final equations as

$$\frac{\partial \bar{\sigma}}{\partial t} + \bar{u} \cdot \nabla_H \bar{\sigma} = \frac{1}{\text{Ra}_e} \left\{ \nabla_H^2 \bar{\sigma} + \frac{2}{105} \text{Ra}_e^2 \delta^2 \nabla_H \cdot [\bar{U}(\bar{U} \cdot \nabla_H \bar{\sigma})] \right\}, \quad (6)$$

$$\nabla_H \cdot (\bar{\sigma} \nabla_H \bar{\Phi}) = 0, \quad (7)$$

$$\nabla_H \cdot \bar{u} = 0, \quad (8)$$

$$\text{Re} \delta^2 \left(\frac{\partial \bar{u}}{\partial t} + \bar{u} \cdot \nabla_H \bar{u} \right) = -\nabla_H \bar{p} + \nabla_H^2 \bar{\Phi} \nabla_H \bar{\Phi} - 3\bar{U} + \delta^2 \nabla_H^2 \bar{u}. \quad (9)$$

Here the overbar denotes depth-averaged quantity, the operator ∇_H denotes the in-plane gradient (to distinguish from the full three-dimensional gradient), and $\bar{U} \equiv \bar{u} - u_\infty$ is the difference between the total depth-averaged velocity and the electroosmotic velocity.

The main contributions of this new equation set are the Taylor-dispersion-type term in the conductivity equation, and the Darcy-Brinkman-Forchheimer (DBF) type of momentum equation which is of second-order consistency in δ (Chen et al., 2004; Liu and Masliyah, 1996). We present preliminary results in the assessment of the validity and accuracy of the model.

Figure 4 compares the linear stability results for growth rate of disturbances versus wave number at a single Rayleigh number of $\text{Ra}_e = 5.000$. We perform linear analyses using the following three models:

1. The linear integrated momentum equations used by Storey et al. (2004).
2. The linearized three-dimensional equations (Lin et al., 2004).
3. The depth-averaged DBF formulation presented here.

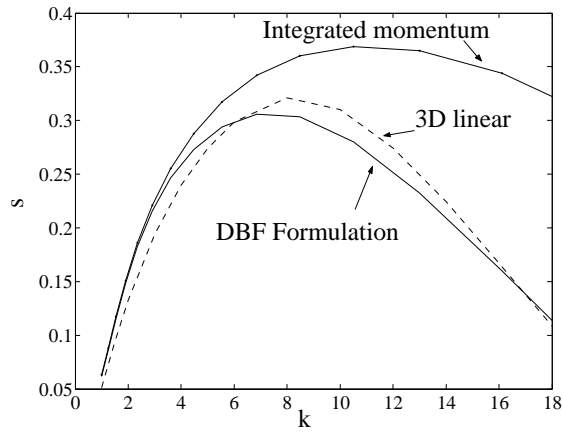


Figure 4. Comparison of growth rates of disturbances as predicted by three models. Shown here are the real part of the growth rates versus the wave number for $Ra_e = 5.000$ as computed with the DBF momentum equation presented here, the integrated momentum equation (δ^0 approximation, Storey et al., 2004), and the three-dimensional equation set. The DBF formulation represents in-plane viscous stresses that quench the unphysically high wave number growth and is in agreement with the three-dimensional result.

Note that at the linear regime, the Taylor dispersion in Eq. (6) drops as a higher-order term, and the only difference between the models are within the momentum equations. We find that all three models are in good agreement for wave numbers below about 4. However, when compared with the more accurate three-dimensional analysis, the DBF momentum equation provides significantly better results at higher wave numbers than the lower-order, integrated momentum approximation.

The characteristics of the DBF momentum equations also make it more advantageous to use in nonlinear simulations when compared with the integrated momentum equation. In particular, the inclusion of in-plane diffusion $\delta^2 \nabla_H^2 \bar{u}$ preserves a mathematical structure similar to the original Navier-Stokes equations, and enables reproduction of the boundary effects (*e.g.*, at $y = \pm 1$ walls) that are not captured by lower-order approximations. This will be discussed further in a future work, and here we simply show some sample results of the full nonlinear, depth-averaged simulations with Eqs. (6–9). That is, a model with the combined effects of Taylor dispersion and the DBF momentum equation. We try to reproduce the experimental image presented in Fig. 1 at the two lower voltages (25,000 and 50,000 V/m); the result is shown in Fig. 5. Again the model reproduces essential features observed in the experiments such

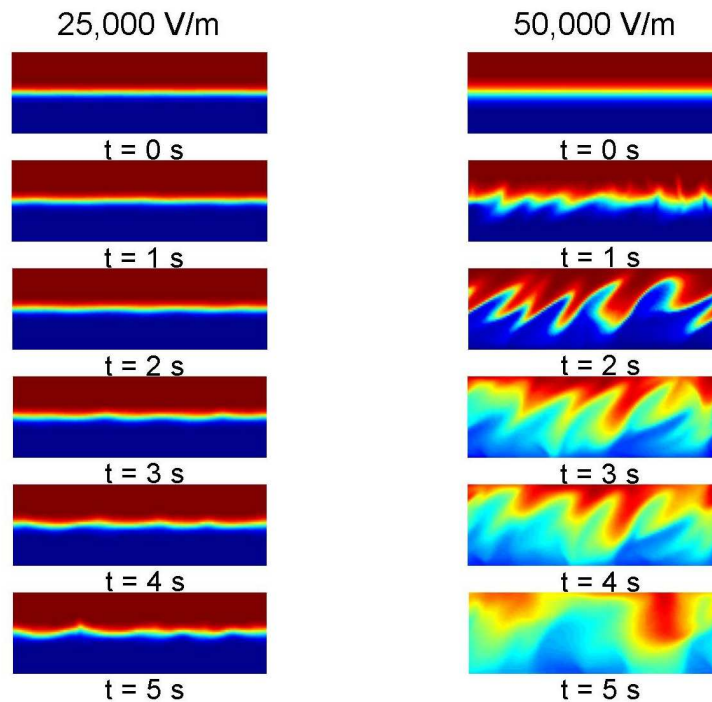


Figure 5. Nonlinear simulation of the depth-averaged equation system. This model includes the combined effects of the Taylor dispersion and the DBF momentum equation. In the strongly nonlinear regime the Taylor dispersion acts as an extra smoothing mechanism. The results compare favorably with the experimental data presented in Fig. 1.

as the fastest growing wave numbers and the growth rates of the interface disturbance amplitude. However, note that the computations are now at exactly the same field strength as those applied in the experiments (as opposed to the unnaturally low fields used for comparison with the simple 2D model results of Fig. 3). Future work will also include the application of the model to different flow configurations such as those used in field amplified sample stacking (FASS).

6. Summary

In this work we have presented experimental, numerical, and analytical results that explain the basic mechanisms behind an electrokinetic mixing phenomenon observed in microfluidic channels. We have presented analysis and computations based on various sets of assumptions for electrokinetic flows in a long, thin channel with a transverse conduc-

tivity gradient. Our models are able to predict general trends in the data, as well as many of the qualitative and quantitative aspects of the observed flow field. Ongoing work includes the development of a generalized, depth-averaged model for a wide class of electrokinetic flows (such as FASS) in thin microfluidic channels.

The models presented in this work are useful in optimization studies, as parameter space can be spanned in simulations more quickly than in the laboratory. The results described by Oddy et al. (2001) has demonstrated that oscillatory electric field can potentially drive even more vigorous mixing. The models presented here can be used to optimize the form of the forcing function, to design the shape of a micro-mixer, and to develop optimal control strategies for both the micro-mixing and the suppression of instabilities.

Acknowledgments

This work was sponsored by DARPA (Contract Number F30602-00-2-0609) with Dr. Anantha Krishnan as contract monitor and by an NSF CAREER Award (J.G.S.) with Dr. Michael W. Plesniak as contract monitor.

References

- [1] J. Baygents, F. Baldessari, Electrohydrodynamic instability in a thin fluid layer with an electrical conductivity gradient, *Phys. Fluids*, Vol.10, 1, 301–311, 1998.
- [2] C.-H. Chen, J.G. Santiago, Electrokinetic instability in high concentration gradient microflows, *Proceedings of IMECE-2002*, CD Vol.1, #33563, 2002.
- [3] C.-H. Chen, H. Lin, S.K. Lele, J.G. Santiago, Convective and absolute electrokinetic instability with conductivity gradients, *J. Fluid Mech.*, in press, 2004.
- [4] J.F. Hoberg, J.R. Melcher, Internal electrohydrodynamic instability and mixing of fluids with orthogonal field and conductivity gradients, *J. Fluid Mech.*, Vol.73, 333, 1976.
- [5] H. Lin, B.D. Storey, M.H. Oddy, C.-H. Chen, J.G. Santiago, Instability of electrokinetic microchannel flows with conductivity gradients, *Phys. Fluids*, Vol.16(6), 1922–1935, 2004.
- [6] S. Liu, S. Masliyah, Single fluid flow in porous media, *Chem. Eng. Comm.* Vol.148–150, 653–732, 1996.
- [7] J.R. Melcher, G.I. Taylor, Electrohydrodynamics: a review of the role of interfacial stresses, *Annu. Rev. Fluid. Mech.*, Vol.1, 111–146, 1969.
- [8] M.H. Oddy, J.G. Santiago, J.C. Mikkelsen, Electrokinetic instability micromixing, *Anal. Chem.*, Vol.73, 5822–5832, 2001.
- [9] R.F. Probstein, *Physicochemical Hydrodynamics*, John Wiley & Sons, New York, 1994.
- [10] B.D. Storey, B.S. Tilley, H. Lin, J.G. Santiago, Electrokinetic instabilities in thin microchannels, *Phys. Fluids*, in review, 2004.